

# AN UNSTEADY AND TIME-AVERAGED STUDY OF A GROUND VORTEX FLOW

N J Lawson\*, J M Eyles\*\*, K Knowles\*\*

\*College of Aeronautics, Cranfield University, Cranfield MK43 0AL, UK

\*\*Dept. of Aerospace, Power & Sensors, Cranfield University, Shrivenham SN6 8LA, UK

**Keywords:** *ground vortex, compressible flow, PIV*

## Abstract

PIV and LDA results are presented from a scaled compressible ground vortex flow with a moving ground plane. PIV data are recorded from the ground vortex about the jet centreline, over a range of nozzle pressure ratios (NPRs) from 2.3 - 3.7, nozzle height to diameter ratios ( $h/d_n$ ) from 3 - 10 (where  $d_n = 12.7\text{mm}$ ) and cross flow velocities ( $V_\infty$ ) from 10 - 20 m/s, corresponding to effective velocity ratios of  $19 < V_e^{-1} < 38$ . LDA data is also recorded about the time-averaged vortex centre and compared to cinematic sequences of PIV vector maps. The analysis shows the ground vortex position to fluctuate chaotically in the freestream and vertical planes by rms distances of  $4.47d_n$  and  $2.18d_n$  respectively. Time averaged data suggested the ground vortex position to be most sensitive to changes in cross flow velocity as consistent with the effective velocity scaling parameter  $V_e^{-1}$ .

## 1 Introduction

The ground vortex is a common feature of flow fields generated by short take-off and vertical landing (STOVL) aircraft such as the Harrier and more recently the STOVL variant of the Joint Strike Fighter (JSF) [1,2]. The ground vortex occurs when a jet impinging on a stationary or moving ground plane is subject to a cross flow (see Fig. 1.). It is present over a range of aircraft heights, nozzle pressure ratios and cross flow velocities and is positioned forward of the aircraft, typically extending around it in a horseshoe shape [2,3]. The ground vortex is also highly unsteady, with periodic

shedding of fluid up towards the nozzle exit, causing ingestion issues and power loss [3,4].

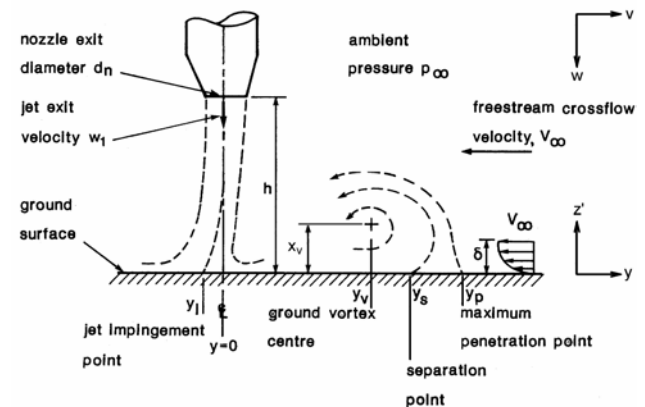


Fig. 1. Ground Vortex Parameters

Previous experimental studies of this type of flow have included water models [5-8] and compressible flow [2,9]. In the former case laser induced fluorescence techniques (LIF) and laser Doppler anemometry (LDA) have been used [5-8]. This work has qualified the ground vortex unsteadiness and more specifically with LDA, has found this unsteadiness to be attenuated with increasing cross flow [7,8].

The former case of compressible flow studies, has seen detailed measurements of ground-plane mean pressure data between effective velocity ratios of 7 - 75, as well as studies on the effect of jet angle [2,9]. Other studies with a low-speed jet have used flow visualisation and hot wire [3]. The use of hot wire allowed spectral analysis of the ground vortex and found low frequency characteristics (5-10Hz) which were attributed to “puffing” or shedding instability from the top of the ground vortex.

Given the limited quantitative data available, there is therefore, an opportunity to apply advanced optical measurement techniques, such as, LDA [10] and particle image velocimetry (PIV) [11] to compressible ground vortex flows. Further, a combination of PIV and LDA will allow detailed time-averaged and temporal analysis of the flow which was not possible from previous studies.

This paper presents PIV and LDA data from a series of ground vortex flows. Mean, and instantaneous PIV results are analysed for a range of nozzle and cross flow conditions, with a moving ground plane and a choked supersonic jet in all the cases tested.

## 2 Experimental Set-up

### 2.1 Wind Tunnel Facility

An open jet wind tunnel (OJWT) with an elliptical working section of 1.14m x 1.52m was used for all the measurements. An in-house rolling road with surface dimensions 1.8m long by 1.2m wide, with boundary layer and belt suction, was also inserted into the working section. The boundary layer suction is positioned immediately before the rolling surface and was adjusted to reduce the boundary layer thickness before measurements were made. This tunnel system provides realistic ground simulation up to 30 m/s.

All measurements were taken using a 12.7mm exit diameter conical convergence nozzle, of length 10 diameters [2,9]. Air to the nozzle, with a pressure of 4 bar, was supplied through a 50.8mm diameter pipe, via a two-part plenum chamber, of size 340mm x 150mm x 140mm. Four additional 12.7mm injection ports were inserted to provide an inlet for the PIV and LDA seeding. Flow straightening gauze was inserted between the two parts of the plenum to improve flow quality.

The freestream was seeded using a JEM Hydrosonic 2000 and an in-house design of seeder, used to provide the jet seeding.. A 5% glycerol/water solution was used as seeding material for the nozzle.

### 2.2 Laser Measurement Systems

The PIV system consisted of a Dantec FlowMap 500 acquisition box and TSI UltraPIV data processing software. The FlowMap system was connected to a Kodak ES1.0 megapixel CCD camera and a New Wave Gemini Nd:YAG double-pulsed laser. The laser and camera were synchronized to run at a maximum frame rate of 15Hz. The camera was mounted on an x-y-z lightweight traverse (see Fig. 2.). PIV images were processed with UltraPIV, using the Hart algorithm [12], with a primary correlation window of 32 x 32 pixels, a sub-correlation window of 16 x 16 pixels and a search radius of 8 x 8 pixels. This yielded vector maps with around 100 x 100 vectors and at a spatial resolution of 2mm x 2mm over a 250mm x 250mm flow area.

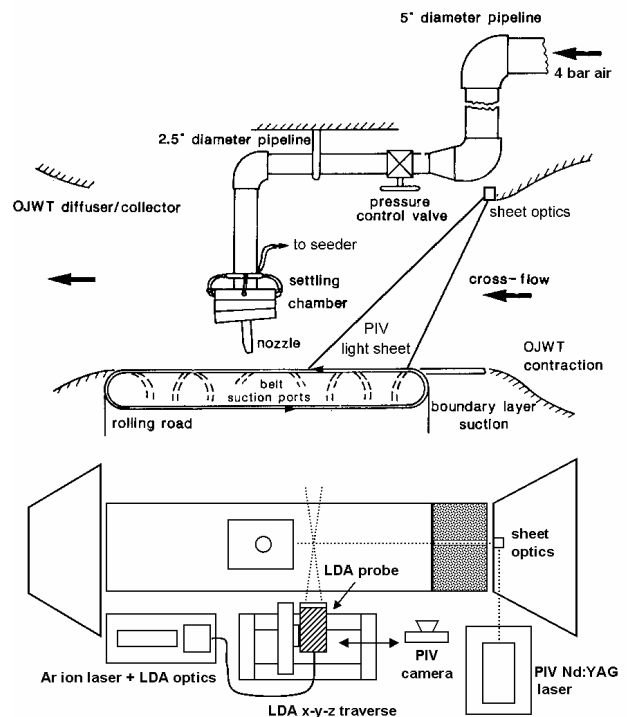


Fig. 2. Experimental Facility

LDA data was recorded using Dantec 2D FibreFlow optics and a pair of BSA Enhanced processors. A focal length of 1m was used with the 514.5nm (green) and 488nm (blue) beams in conjunction with a 1.98x beam expander giving a probe volume of 150 $\mu$ m(z) x 150 $\mu$ m(x) x 5mm(y). The probe optics were

mounted on the same lightweight traverse used for the PIV measurements (see Fig. 2.). Burst resolution was set to 32 and sampling periods were set to a maximum of 60s or a maximum of 10000 samples per point.

### 3 Flow Measurements

PIV data were taken for nozzle pressure ratios (NPRs) between 2 and 4, nozzle height to diameter ratios ( $h/d_n$ ) between 3 and 10 and cross flow velocities ( $V_\infty$ ) between 10 m/s and 20 m/s (see Table 1). In all cases the rolling road was running at the freestream speed. Typically 70 PIV image pairs were recorded for each case as limited by the acquisition box. The instantaneous vector maps were also converted into AVI movies for further qualitative study of the ground vortex.

LDA data were recorded for case 9 at the time-averaged ground vortex core position, as defined by the PIV data.

In a number of the results, the non-dimensional parameter effective velocity ratio  $V_e$  is used for analysis

$$V_e = \sqrt{\frac{1/2 \rho_\infty V_\infty^2}{1/2 \rho_1 w_1^2}} \quad (1)$$

where  $V_\infty$ ,  $w_1$  and  $\rho_1$  are the freestream velocity, nozzle exit velocity and nozzle exit density respectively.

Case	NPR	$h/d_n$	$V_\infty$ (m/s)
1	2.36	3	10
2	2.36	4	10
3	2.36	5	10
4	2.36	7	10
5	2.36	10	10
6	2.36	10	15
7	2.36	10	20
8	3.02	10	15
9	3.72	10	10
10	3.72	10	15

Table 1. Experimental conditions

## 4 Results and Discussion

The following section presents data from the LDA and PIV measurements. The data is presented in two parts, namely, time-averaged data and then transient data, which also includes spectral analysis of the ground vortex core.

### 4.1 Time Averaged Data

With reference to Fig. 3, an example of a time-averaged PIV vector and vorticity map is shown with  $NPR = 3.72$ ,  $h/d_n = 10$  and  $V_\infty = 10$  m/s. The ground vortex is clearly visible, with the vortex core located at  $y/d_n = 15.8$  and  $z'/d_n = 4.35$  and maximum velocity and vorticity magnitudes of around  $V = 25.0$  m/s and  $\xi = 9.0$   $s^{-1}$ .

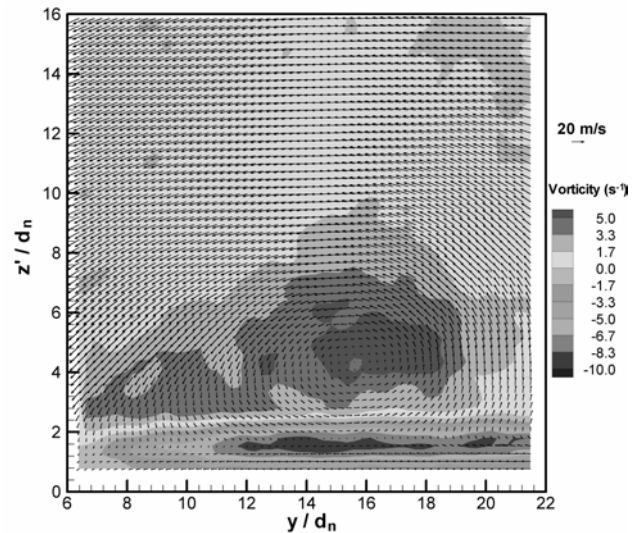


Fig. 3. PIV and Vorticity Vector Map ( $NPR = 3.72$ ,  $h/d_n = 10$ ,  $V_\infty = 10$  m/s)

Further examination shows maximum velocity to occur in the uppermost right hand side of the ground vortex, in the direction of the cross flow. Maximum vorticity occurs at the core of the vortex ( $7.4$   $s^{-1}$ ) and in the shear region between the ground vortex and the wall jet ( $7.4$   $s^{-1}$ ) formed by the jet. Substantial PIV data dropout in the region adjacent to the moving surface, however, caused problems with velocity and vorticity analysis. This data dropout was caused by spurious reflections from the rolling road belt.

4.1.1 Effect of Nozzle Height

Figure 4 shows the effect of nozzle height in terms of  $h/d_n$ , on vortex core position  $y_v/d_n$ ,  $z'_v/d_n$  for a range of  $h/d_n = 3-10$ . The results show the vortex core position to move less than  $2 d_n$  in  $y$  and less than  $1 d_n$  in  $z$  as  $h/d_n$  is increased from 3 to 10. This effect is consistent with the average decay profile of the jet through entrainment [13] and is also reflected in the scaling parameter effective velocity ratio  $V_e^{-1}$  which, primarily considers jet exit velocity  $w_1$  and cross flow velocity  $V_\infty$ . In this case effective velocity ratio is fixed at  $V_e^{-1} = 38.1$ .

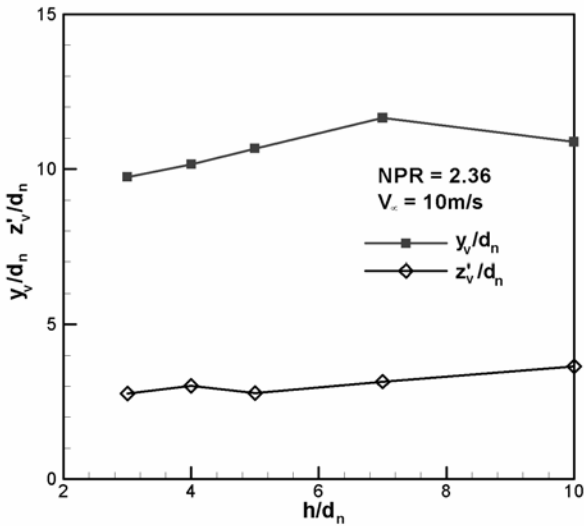


Fig. 4. Effect of  $h/d_n$  on vortex core position  $y_v/d_n$ ,  $z'_v/d_n$  (NPR = 2.36,  $V_\infty = 10$  m/s)

4.1.2 Effect of NPR

The effect of NPR on vortex core position is shown in Fig. 5. In contrast to vortex changes with  $h/d_n$ , it can be seen that in this case there is a significant movement of the mean vortex position. With an NPR range of 2.36-3.72 the vortex moves approximately  $5d_n$  in  $y$  and  $1d_n$  in  $z'$ . Since effective velocity ratio  $V_e^{-1}$  is the key parameter, this high sensitivity in  $y_v$  with NPR would be expected as an increase in NPR will directly increase the exit velocity  $w_1$  with a corresponding increase in  $V_e^{-1}$ . Here the range of  $V_e^{-1} = 25.5 - 32.1$  for NPR = 2.36-3.72. The small change in  $z'$  can be attributed to the self similarity of the wall jet and corresponding changes in thickness with NPR [14].

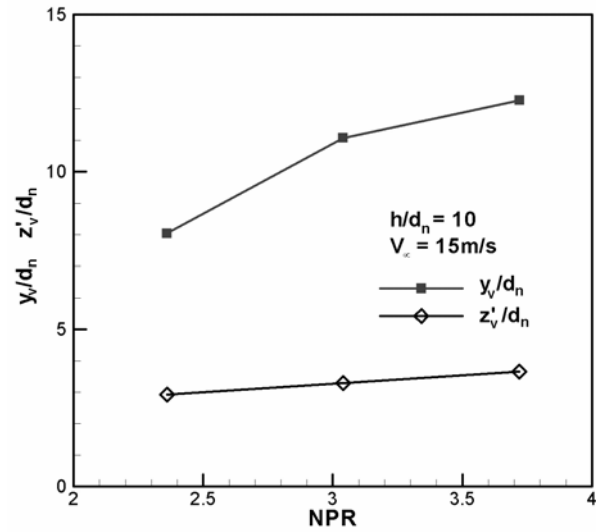


Fig. 5. Effect of NPR on vortex core position  $y_v/d_n$ ,  $z'_v/d_n$  ( $h/d_n = 10$ ,  $V_\infty = 15$  m/s)

4.1.3 Effect of Cross Flow

The effect of cross flow velocity  $V_\infty$  on mean vortex position is shown in Fig. 6. In this case even larger changes in the vortex position occur than for the changes in NPR. Here with a range of cross flow velocities of  $V_\infty = 10-20$  m/s, the mean vortex position moves by more than  $5 d_n$  in  $y$  and  $1d_n$  in  $z'$ . This sensitivity is reflected in the primary parameter, effective velocity ratio  $V_e^{-1}$ , which in this case decreases through a range of  $V_e^{-1} = 38.1 - 19.1$  for  $V_\infty = 10-20$  m/s.

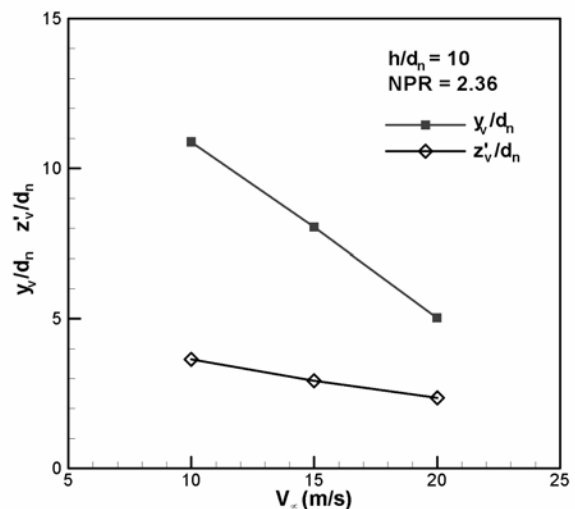


Fig. 6. Effect of cross flow velocity  $V_\infty$  on vortex core position  $y_v/d_n$ ,  $z'_v/d_n$  ( $h/d_n = 10$ , NPR = 2.36)

## 4.2 Transient Data

Transient PIV data were recorded for all the cases outlined in Table 1. Each case yielded 70 vector maps per run and vortex core position were extracted from each vector map using a simple velocity magnitude search in the vortex region. LDA data from case 9, was processed into a spectral distribution using an FFT routine for analysis of the frequency characteristics. This FFT routine was also applied to the equivalent PIV vortex core position time series for comparison with the LDA data.

### 4.2.1 PIV Data

An example of a typical instantaneous PIV vector plot is shown in Fig. 7. If this is compared to the time-averaged result at the same NPR,  $h/d_n$  and  $V_\infty$ , although a vortex core is visible in both cases, the numerous smaller scale vortex structures can be clearly seen in the instantaneous case. These small scale structures are responsible for the unsteady shedding characteristics and large shedding frequency range, reported by previous workers [ref Cim]. The timescale of the small vortices was also found to be less than the PIV camera frame rate, as they could not be tracked from frame to frame. The larger scale vortex structure, however, was present in all PIV frames, but its position was highly transient.

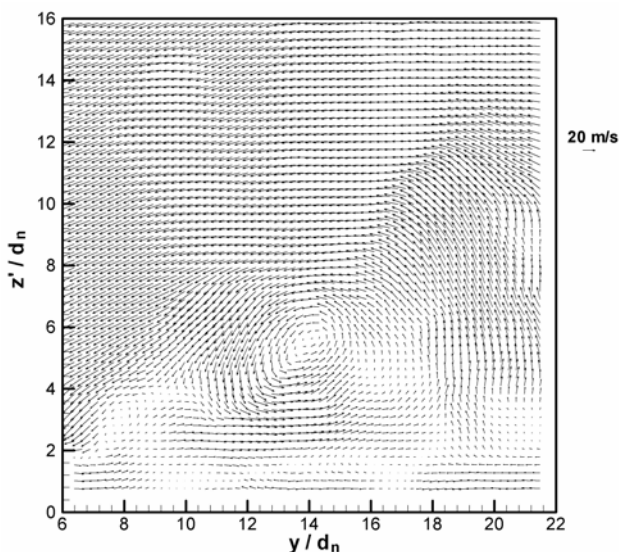


Fig. 7. Example of instantaneous PIV vector plot (NPR = 3.72,  $h/d_n = 10$ ,  $V_\infty = 10$  m/s)

This highly transient characteristic is illustrated in Fig 8. and Fig. 9 which plots the vortex core position from the case illustrated in Fig. 7. The vortex core positions in Fig. 9 correspond to the highlighted section of the time series in Fig. 8.

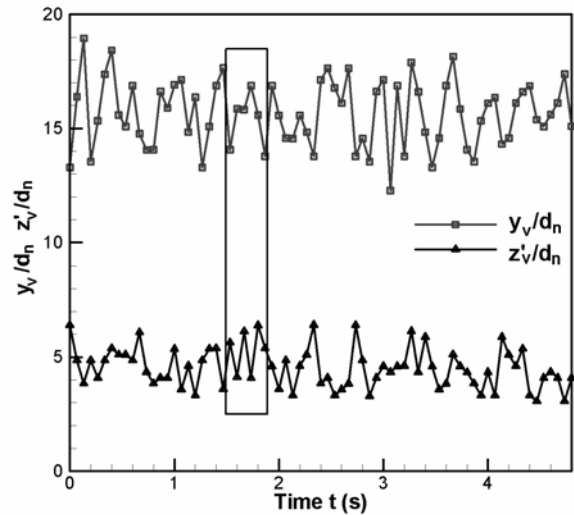


Fig. 8. Vortex core position time series from PIV data (NPR = 3.72,  $h/d_n = 10$ ,  $V_\infty = 10$  m/s)

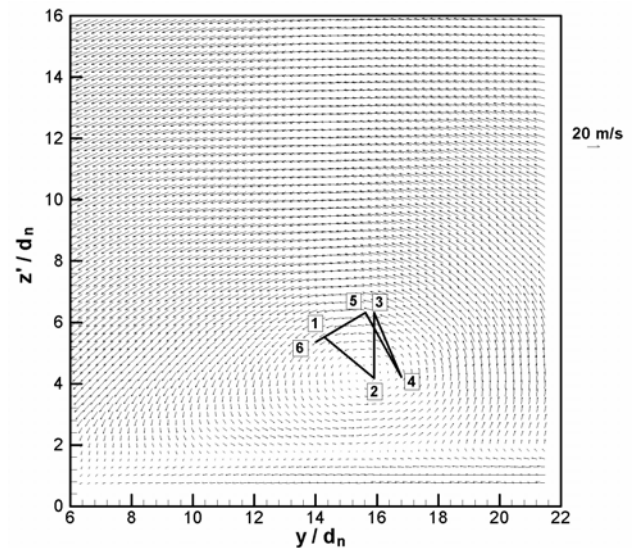


Fig. 9. Vortex core position overlaid on time-averaged PIV vector plot (NPR = 3.72,  $h/d_n = 10$ ,  $V_\infty = 10$  m/s)

The PIV data clearly shows the vortex to have highly chaotic behaviour with no obvious dominant frequency of oscillation. Initially, the plot in Fig. 8 suggests vortex growth and collapse as the core positions towards and away from the nozzle exit, since the  $y_v$  amplitudes are

the greatest ( $y_{rms}/d_n = 4.47$ ,  $z'_{rms}/d_n = 2.18$ ). The chaotic behaviour, however, is further highlighted in the spectral plot of the PIV time series shown in Fig. 10. Here peak spectral amplitudes occur at around 3Hz and 4Hz but no single frequency or harmonic is present within the frequency resolution of the PIV system. This is limited to 7.5Hz due to the 15Hz frame rate of the CCD camera. Increased temporal resolution can be obtained by analysis of LDA which has sampling rates of the order of kHz. These results will now be presented.

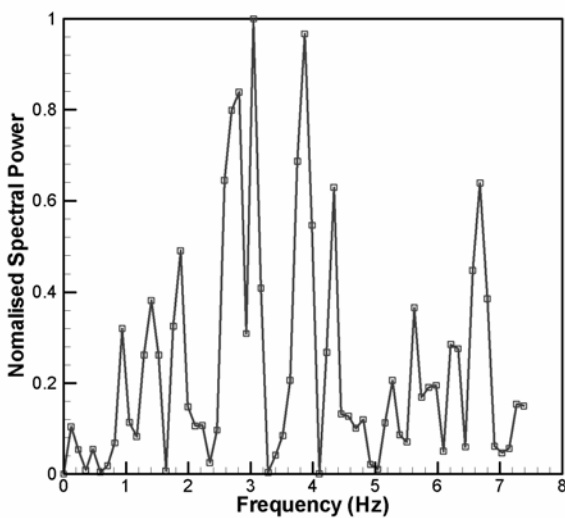


Fig. 10. PIV spectral distribution (NPR = 3.72,  $h/d_n = 10$ ,  $V_\infty = 10$  m/s)

#### 4.2.2 LDA Data

LDA time series and spectral data taken from the vortex core time-averaged position are shown in Fig. 11 and Fig. 12 for NPR = 3.72,  $h/d_n = 10$  and  $V_\infty = 10$  m/s with a sample size of 10000. The LDA data rate was around 1kHz. In this case the time-averaged velocity is  $v = 0.519$  m/s and the rms velocity is  $v_{rms} = 8.75$  m/s or 87.5% of free stream. Peak velocities, however, were up to 25 m/s or 2.5 times free stream velocity indicating the highly transient nature of the flow.

Examination of the spectral distribution in Fig. 12 shows the majority of the spectral power to occur below 5 Hz. This is consistent with the PIV results shown in Fig. 10. As the frequency resolution for the LDA is significantly higher though, the results show

that there is still a significant amount of power up to around 30Hz. Average spectral amplitude above 45Hz then decays to less than 10% of the peak amplitude suggesting less influence of the smaller, higher frequency vortex structures in this region.

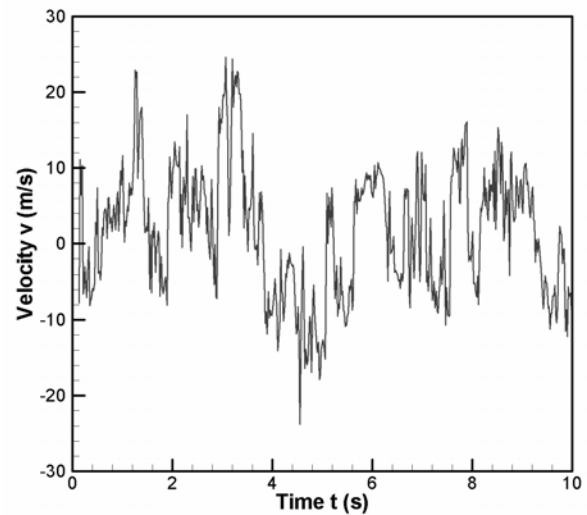


Fig. 11. Vortex core  $v$  velocity time series from LDA data (NPR = 3.72,  $h/d_n = 10$ ,  $V_\infty = 10$  m/s)

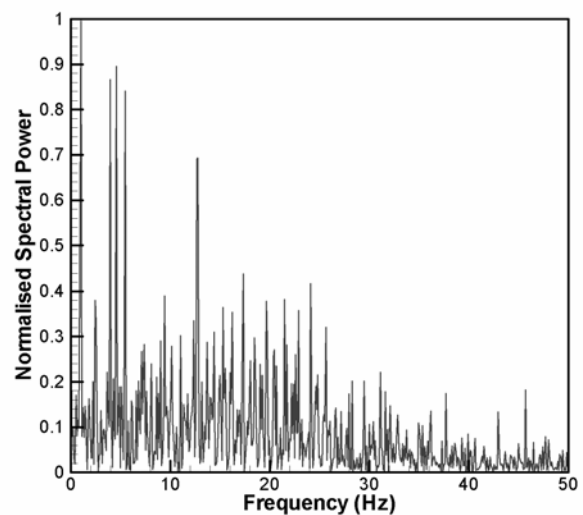


Fig. 12. LDA spectral distribution (NPR = 3.72,  $h/d_n = 10$ ,  $V_\infty = 10$  m/s)

#### 4.3 Further Work

Given the findings of the LDA spectral analysis, a higher frame rate PIV system is required to analyse the ground vortex structures in the core region. As a minimum, the frame rate must be increased to 50-60Hz. Given that the shear

instabilities of the main jet are in the order of kHz, a more suitable minimum sampling rate of 1-2kHz would be desirable. This requirement is now well within the specifications of commercially available time-resolved PIV systems, based on CMOS imaging cameras and Nd:YLF double pulsed lasers. Cranfield University will shortly acquire such a system and therefore, plans to apply it to this flow regime.

#### **4 Conclusions**

PIV and LDA data have been presented from a scaled compressible ground vortex flow, representative of the flow regime, encountered by a STOVL aircraft in ground effect.

Analysis of the time-averaged PIV data has shown the ground vortex to be most sensitive to changes in cross flow velocity ( $V_\infty$ ) and NPR and to be least sensitive to changes in nozzle height ( $h/d_n$ ). The instantaneous PIV results have also shown the ground vortex to fluctuate chaotically by rms movements of up to  $y_{rms}/d_n = 4.47$  and  $z'_{rms}/d_n = 2.18$ . No dominant period of oscillation was apparent in the PIV spectral analysis and this was confirmed in further spectral analysis of LDA data taken from the mean vortex core. Both results show the majority of the spectral energy to occur up to 30 Hz. Further work using a kHz time-resolved PIV system is planned to further analyse the highly transient ground vortex structures.

#### **References**

- [1] Knowles K., Bray D., Bailey P.J. and Curtis P. "Impinging jets in cross flow", *The Aeronautical Journal of the Royal Aeronautical Society*, 92, 952, pp 47-56, February 1992.
- [2] Knowles, K. and Bray D., "Ground Vortex Formed by Impinging Jets in Crossflow", *J. Aircraft*, 30 (6), pp 872-878 (1993)
- [3] Cimbala J.M., Billet M.L., Gaublumme D.P. and Oefelein J.C. "Experiments on the Unsteadiness Associated with a Ground Vortex", *J. Aircraft* 28 (4), pp 261-267 (1991)
- [4] Kuhn R.E. "Design Concepts for Minimizing Hot-Gas Ingestion in V/STOL Aircraft", *J. Aircraft* 19 (10), pp 845-850 (1982)
- [5] Behrouzi, P. and McGuirk, J.J., "Capture of Unsteady Flow Features in Re-ingestion Flows Using a Laser-Induced Fluorescence (LIF) Technique", *Procs Optical Methods and Data Processing in Heat and Fluid Flow*, April 1996, City University, London, UK, pp 429-438 (1996)
- [6] Behrouzi, P. and McGuirk, J.J. "Experimental Data for CFD Evaluation of Jets with or without Cross Flow Effects for ASTOVL Flow Application", *AGARD Conference Proceedings 534, Computational and Experimental Assessment of Jets in Cross flow*, Winchester, April 1993, pp 8.1-8.11 (1993)
- [7] Barata J.M.M., Durao D.F.G., Heitor M.V., McGuirk J.J. "The Turbulence Characteristics of the Single Impinging Jets Through a Crossflow" *Proceedings of the 6<sup>th</sup> Symposium on Turbulent Shear Flows*, Toulouse, France, September 1987 (1987)
- [8] Barata J.M.M., Durao D.F.G., McGuirk J.J. "Numerical Study of Single Impinging Jets Through a Crossflow", *J. Aircraft* 26 (11), p1002-1008 (1989)
- [9] Bray, D., "Jets in Cross-flow and Ground Effect", PhD Thesis, Cranfield University, RMCS Shrivenham, UK (1992)
- [10] Durst F., Melling A. & Whitelaw J.H., "Principles and Practice of Laser Doppler Anemometry", Second Edition, London; New York: Academic Press (1981)
- [11] Adrian R.J., "Particle-imaging techniques for experimental fluid mechanics," *Annu. Rev. Fluid Mech.* 23, pp 261-304 (1991)
- [12] Hart D.P., "PIV Error Correction", in *Laser Techniques Applied to Fluid Mechanics*, Springer-Verlag, Berlin, New York, ISBN 3-540-66738-5, pp 19-35 (2000)
- [13] Lau J.C., Morris P.J. & Fisher M.J., "Measurements in subsonic and supersonic free jets using a laser velocimeter" *J.Fluid Mech* 93(1), p1-27 (1979)
- [14] Knowles K. and Myszko M. "Turbulent measurements in radial wall-jets", *Experimental Thermal and Fluid Sciences* 17, pp 71-78 (1998)